Divergent performances of vegetation indices in extracting photosynthetic phenology for northern deciduous broadleaf forests

Yajie Yang, Rui Chen, Gaofei Yin, *Senior Member*, Cong Wang, Guoxiang Liu, Aleixandre Verger, Adrià Descals, Iolanda Filella, and Josep Peñuelas

Yajie Yang, Rui Chen and Gaofei Yin are with the Faculty of Geosciences and Environmental Engineering, Southwest Jiaotong University, Chengdu, 610031, China. (e-mail: yingf@swjtu.edu.cn).

Cong Wang is with the Key Laboratory for Geographical Process Analysis & Simulation of Hubei Province/School of Urban and Environmental Sciences, Central China Normal University, Wuhan 430079, China.

Guoxiang Liu is with the Faculty of Geosciences and Environmental Engineering, Southwest Jiaotong University, and the State-Province Joint Engineering Laboratory of Spatial Information Technology for High-Speed Railway Safety, Chengdu 610031, China.

Aleixandre Verger is with the Desertification Research Centre CIDE-CSIC, València 46113, Spain.

Adrià Descals, Iolanda Filella and Josep Peñuelas are with CREAF, Cerdanyola del Vallès, Barcelona 08193, Catalonia, Spain, and also with CSIC, Global Ecology Unit CREAF‑CSIC‑UAB, Bellaterra, Barcelona 08193, Catalonia, Spain.

Abstract

Accurate estimation of photosynthetic phenology is of great importance for understanding carbon cycles. Most vegetation indices (VIs) calculated from remotely sensed reflectances represent the canopy structure and have high uncertainty in detecting the real photosynthetic phenology. We compared the start/end of the photosynthetically active season (SOS/EOS) extracted from the normalized difference vegetation index (NDVI), the enhanced vegetation index (EVI), the near-infrared reflectance of vegetation (NIRv) and the product of NIRv and solar incident radiation (NIRvP) over northern deciduous broadleaf forests, using the metrics from solar-induced chlorophyll fluorescence (SIF), a proxy for photosynthesis, as reference. We found that the growing season extracted from the structural VIs was generally longer than the real duration of photosynthetic activity retrieved from SIF: the timing of SoS derived from NDVI < NIRvP < EVI ≈ NIRv ≈ SIF and the timing of EOS from NDVI > NIRv ≈ EVI > NIRvP ≈ SIF. We accounted for the mechanism underlying these phenological discrepancies using the paradigm of light-use efficiency. The sensitivity of the Vis to the main factors limiting photosynthesis differed across VIs and the contribution of these factors to the phototsynthetic phenology also vary across growth stages: EVI and NIRv are sensitive to chlorophyll content and the fraction of absorbed photosynthetically active radiation absorbed by chlorophyll (FAPAR$_{chl}$) appears as the dominant factor of spring photosynthetic phenology, while NIRvP is a good proxy of the total amount of photosynthetically active radiation absorbed by chlorophyll (APAR$_{chl}$) which is is key in autumn when radiation determines photosynthetic phenology. We therefore suggest that VIs should be dedicatedly selected to improve the extraction of photosynthetic phenology: EVI and NIRv for accurate retrieval of the timing of SOS, and NIRvP for the EOS.

Index Terms—Photosynthetic phenology, deciduous broadleaf forest, vegetation indices, light-use efficiency

I. INTRODUCTION

The annual growth and uptake of photosynthetic carbon by Northern deciduous broadleaf forests (DBFs) have strong seasonal cycles, which substantially influences the annual and interannual variation of atmospheric CO_2 concentrations [1]. Climatic warming has lengthened the growing season and increased the uptake of photosynthetic carbon by DBFs [2]. A better understanding of the photosynthetic phenology of DBFs is therefore necessary for more accurate predictions of future climate.

Satellite observations can provide spatiotemporally continuous reflectances over terrestrial surfaces. Most vegetation indices (VIs) extracted from satellite reflectances contain information about biomass greenness and have therefore been widely used to monitor large-scale terrestrial-surface phenology, which has greatly improved our understanding of seasonal productivity in recent decades [3]. Greenness VIs are generally reliable proxies for tracking the dynamics of gross primary productivity (GPP) but by nature represent vegetation structure, i.e., potential GPP,

and cannot be directly converted to actual GPP, because plant photosynthesis is also constrained by environmental stress, as expressed by environmental scalars in models of light-use efficiency (LUE) [4].

The performances of VIs in identifying the interannual variation in photosynthetic phenology remain highly uncertain [3]. For example, the commonly used normalized difference vegetation index (NDVI) scales well with the fraction of absorbed photosynthetically active radiation (FAPAR) but substantially overestimates the length of photosynthetic phenology derived from tower-based measurements of GPP [5] indicating a systematic bias in seasonality between plant structure and function [3]. In comparison, the enhanced vegetation index (EVI) is more sensitive to FAPAR absorbed by chlorophyll (FAPAR$_{chl}$) [6], so EVI outperforms NDVI, because chlorophyll is a robust proxy for foliar photosynthetic capacity [7]. Another study, however, found that the length of the photosynthetically active season derived from EVI also overestimated the actual active season in deciduous broadleaf forests by two weeks [8]. The near-infrared reflectance of vegetation (NIRv) [9], another popular VI in the phenological community, performed comparably with EVI in extracting photosynthetic phenology [3]. NIRvP, expressed as the product of NIRv and solar incident radiation, is an improved version of NIRv and is a robust structural proxy of GPP [10]. Its performance in extracting photosynthetic phenology, however, remains unknown.

Solar-induced chlorophyll fluorescence (SIF) is a small part of the 650-680 nm electromagnetic signal re-emitted by chlorophyll after absorbing sunlight during photosynthesis and can be directly detected by satellite sensors [11]. In contrast to information about green biomass identified by structural VIs, SIF is mechanistically linked with photosynthesis and therefore can respond quickly to nearly all factors regulating photosynthetic activity [11] [12]. SIF therefore has the promising potential to track the seasonal changes in plant photosynthesis. Many recent studies have demonstrated the rationality of using SIF in extracting photosynthetic phenology, and the results can be used as reference values to validate the performance of VIs [5] [12].

In summary, commonly used VIs were designed to represent plant structure rather than physiology, so the derived phenology characterized the seasonal variation in potential GPP, which systematically overestimates the actual GPP. Very few studies have been devoted to comparing the photosynthetic phenology extracted from structural VIs, especially from the newly developed VIs. We compared the start and end of the photosynthetically active season in northern DBFs using NDVI, EVI, NIRv and NIRvP, using the SIF results as reference. The specific scientific questions are twofold: (1) does the terrestrial-surface phenology derived from structural VIs exhibit a systematic bias compared with photosynthetic phenology of DBFs and (2) what is the underlying mechanism?

II. MATERIALS AND METHODS

A. Study Area

This study focused on the northern (≥30°N) DBFs, which are generally in regions with moist, warm summers and frosty winters, in three main areas: (1) eastern North America, (2) western and central Europe and (3) eastern Asia. The leaves unfold in spring as temperatures increase, senesce and then fall in autumn with the shortening of the photoperiod and the declining of the tempreture [5].

B. Data sets and Indices

MODIS: The VIs were calculated using surface reflectance from the MCD43A4 Version 6 product, which is adjusted to nadir from multi-angular, cloud-free, atmospherically corrected measurements using a bidirectional reflectance distribution function (BRDF) for the solar angle at local noontime [13]. MCD43A4 is produced daily based on 16 d retrieval period of Terra and Aqua MODIS data at a resolution of 500 m. Low-quality (magnitude BRDF inversions) and snow-contaminated observations were removed before analysis based on the quality flag.

GOSIF: GOSIF, with a spatial resolution of 0.05 × 0.05° and a revisit time of 8 d, was used as a reference to extract photosynthetic phenology. It was produced by a machine-learning method using discrete OCO-2 SIF, MCD43C4 reflectance and MERRA-2 meteorological data as inputs. The strong correlation between GOSIF and GPP has been verified at 91 FLUXNET sites around the world (R^2 = 0.73, p < 0.001) [14].

ERA5-Land: The solar incident radiation (also known as shortwave radiation) provided by ERA5-Land was used to represent the photosynthetically active radiation (PAR). ERA5-Land is the fifth generation of climate reanalysis dataset produced by the European Centre for Medium-Range Weather Forecasts (ECMWF), with a spatial resolution of 0.1° and a temporal resolution of 1 hour [15]. The daily maximum was selected to represent daily value.

CCI land cover: The land-cover products released by the Land Cover Climate Change Initiative (CCI) of the European Space Agency provides global land-cover maps at a spatial resolution of 300 m on an annual basis [16]. CCI divides the terrestrial surface into 22 classes, which have been defined using the United Nations Food and Agriculture Organization's Land Cover Classification System. We delineated DBF whose land type has not changed from 2001 to 2020.

Selected indices: We selected four commonly used VIs for comparing their performances in extracting photosynthetic phenology. They were computed using MODIS reflectances and ERA5 data. The formulations of the VIs are presented in TABLE I.

TABLE Ⅰ
DEFINITION OF THE VEGETATION INDICES TESTED IN THIS STUDY

Vegetation index	Reference
$NDVI = \dfrac{NIR - R}{NIR + R}$	[17]
$EVI = 2.5 \cdot \dfrac{NIR - R}{NIR + 6R - 7.5B - 1}$	[18]
$NIRv = \dfrac{NIR - R}{NIR + R} \cdot NIR$	[9]
$NIRvP = \dfrac{NIR - R}{NIR + R} \cdot NIR \cdot PAR$	[10]

R, *B* and *NIR* are the MODIS reflectances at the red, blue and near-infrared bands, respectively. Photosynthetically active radiation (PAR) is represented by ERA5 shortwave radiation.

C. Extraction of Phenology

Our study period was from 2001 to 2020, representing maximum temporal overlaps of all data sets used. We first aggregated the VIs derived from MODIS and ERA5 data into a resolution of 0.05 × 0.05° and 8 d through an averaging method. The VIs values for different years were averaged every 8 d to obtain their annual climatologies. We then used three methods, Savitzky-Golay (SG), asymmetric Gaussian (AG) and double logistic (DL), to smooth the climatological data. SG filtering is a quadratic fitting method based on the local characteristics of a curve. We set the half-window to 32 d to ensure a high degree of smoothness. Both the AG and DL methods perform least-square fitting to the data with corresponding functions and use the fitted curve to replace the original time series. Detailed information about the three methods are provided by [19]. Smoothing was implemented using TIMESAT software [19].

The start of the photosynthetically active season (SOS) and the end of the photosynthetically active season (EOS) were then extracted using the dynamic-threshold method [19]. Specifically, we adopted the threshold of 50% of the annual amplitude. SOS occurs when the left side of the reconstructed time-series curve before the annual maximum has reached half the amplitude, counted from the base level. EOS is defined similarly, but for the right side of the curve after the annual maximum. The SOS and EOS values extracted from the reconstructed climatologies of VIs and SIFs with the three smoothing methods, i.e., SG, AG and DL, were averaged at pixel scale to obtain robust estimates of phenology metrics.

D. Model of Light-Use Efficiency

We interpreted the divergent performances of the VIs using the LUE paradigm. LUE assumes that plant photosynthesis is jointly controlled by changes in PAR, FAPAR absorbed by chlorophyll ($FAPAR_{chl}$) and LUE [4], i.e., GPP = PAR × $FAPAR_{chl}$ × LUE = $APAR_{chl}$ × LUE, where $APAR_{chl}$ is the amount of PAR absorbed by chlorophyll, i.e., PAR × $FAPAR_{chl}$.

At the seasonal scale, PAR is directly associated with the solar zenith angle and cloud cover, $FAPAR_{chl}$ depends on canopy structure and amount of foliar chlorophyll and LUE denotes LUE under a specific environment at the canopy scale and may vary with factors such as the phenological period (LUE shows diurnal, seasonal and long term variations), physiological conditions (e.g., nutrient levels) and climatic conditions (temperature and water stress) [20].

III. Results

The spatial distribution of the temporal mismatches among the phenological metrics of northern DBFs based on the VIs is shown in Fig. 1. SOS generally had smaller mismatches across all indices compared with EOS, with histograms

centered near zero (Fig. 2 (a)). NDVI- and NIRvP-derived estimates of SOS were an average of 11 d and 6 d earlier than the SIF-derived estimates, respectively. EVI- and NIRv-derived SOSs were very similar and were only 2 d earlier than the reference values. The differences in EOSs across all indices were very distinct, with histograms centered far from zero. NIRvP was the only exception (Fig. 2 (b)). NDVI-, EVI- and NIRv-derived estimates of EOS averaged 42, 14, 13 d later than the SIF-derived estimates, whereas NIRvP performed very well in extracting EOSs, with a bias of only -2 d indicating earlier EOS for NIRvP than SIF.

We further compared the timing of the phenological metrics by latitude (Fig. 3). We considered the range of latitudes 30-60º N where the most part of DBFs are located (Fig. 1). SOSs from all indicators had good consistency at mid-low latitudes (30-40°N) (Fig. 3 (a)). SOS from each index occurred later as latitude increased. Averaged SOSs derived from SIF, EVI, NIRv, NIRvP and NDVI at high latitudes (50-60°N) were about 40, 36, 34, 29 and 17 d later than those at mid-low latitudes, respectively. The divergence of VI-derived SOS, compared with the SIF-derived reference, correspondingly increased with latitude. NDVI- and NIRvP-derived SOSs at high latitudes had larger deviations from SIF-derived SOS, and their estimated SOSs were 24 and 13 d earlier than that estimated by SIF, respectively. EVI-derived SOS nearly coincided with NIRv-derived SOS and occurred only about 4 d earlier than SIF-derived SOS at high latitudes. In contrast, EOS in autumn from all indicators advanced as the latitude increased (Fig. 3 (b)). NIRvP-derived EOS approximated the SIF-derived EOS very well, especially at high latitudes, with a bias of only 1 d. EVI- and NIRv-derived EOSs were comparable, about 15 d later than SIF-derived EOS at high latitudes. As for NDVI-derived EOS, an averaged 41 d lag across all the latitude bands, compared with SIF-derived one, was observed. However, the latitudinal gradient of EOS was not detected from NDVI.
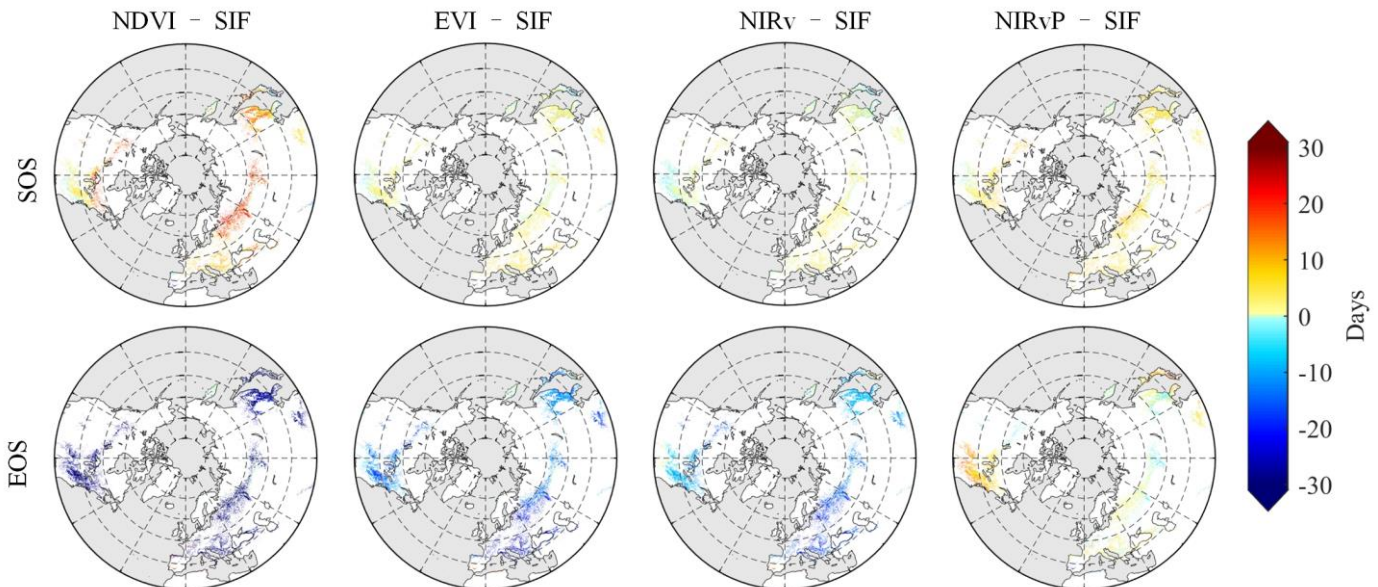
Fig. 1. Spatial distribution of temporal mismatches between phenological metrics derived from the vegetation indices and those from sun-induced fluorescence (SIF). The normalized difference vegetation index (NDVI), enhanced vegetation index (EVI), near-infrared reflectance of vegetation (NIRv) and near-infrared reflectance of vegetation multiplied by incoming sunlight (NIRvP) were used to estimate the start and end of the growing season (SOS and EOS)
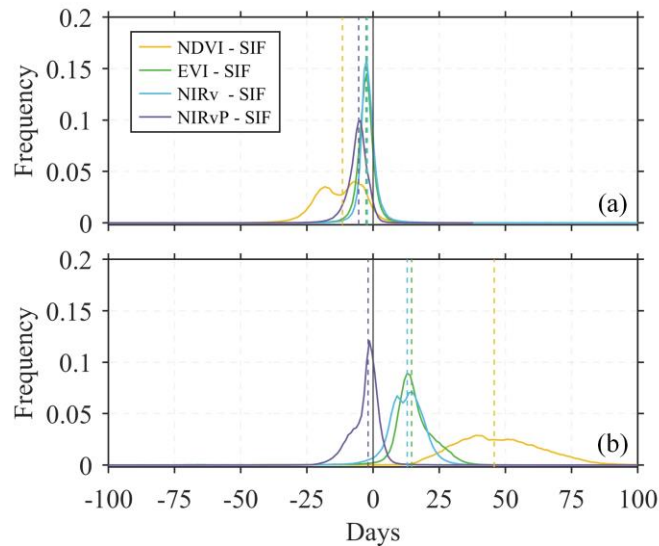
Fig. 2. Frequency distribution of temporal mismatches between phenological metrics derived from the vegetation indices and those from sun-induced fluorescence (SIF). The normalized difference vegetation index (NDVI), enhanced vegetation index (EVI), near-infrared reflectance of vegetation (NIRv) and near-infrared reflectance of vegetation multiplied by incoming sunlight (NIRvP) were used to estimate the (a) start and (b) end of the growing season (SOS and EOS).
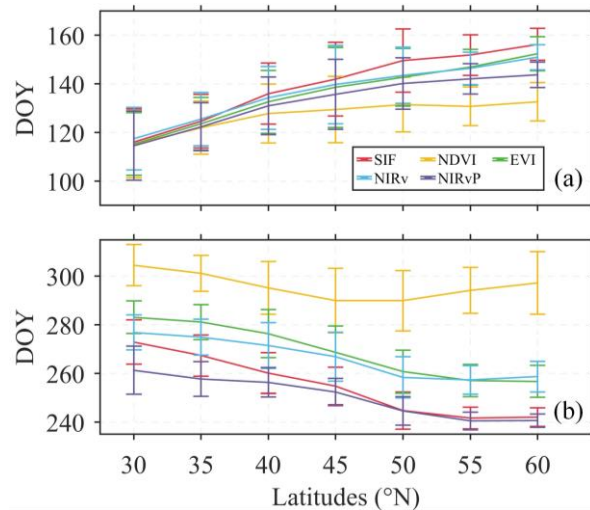

Fig. 3. Latitudinal distribution of averaged (a) start and (b) end of the growing season derived from sun-induced fluorescence (SIF), normalized difference vegetation index (NDVI), enhanced vegetation index (EVI), near-infrared reflectance of vegetation (NIRv) and near-infrared reflectance of vegetation multiplied by incoming sunlight (NIRvP). Error bars indicate regional standard deviations. DOY: day of year.

IV. Discussion

VIs extracted from reflectances have been widely used to estimate photosynthetic phenology. We found deviations in the photosynthetic phenology extracted by different VIs over the northern DBFs (Figs. 1-3). The physical interpretation of VIs and their divergent performances in tracking photosynthetic phenology can be explained using the LUE paradigm. NDVI is widely used as a robust proxy of FAPAR [21], [22], but not all PAR absorbed by a canopy can be used for photosynthesis. PAR at the canopy scale will be absorbed by both chlorophyll and non-photosynthetic vegetation (e.g., stems, branches and senescent leaves) [6], [23]. Only the light absorbed by chlorophyll forces photosynthesis. EVI, the proxy of $FAPAR_{chl}$, was therefore preferred for estimating GPP in recent studies [6] [23]. EVI has been strongly correlated with $FAPAR_{chl}$ (R^2 = 0.97) [23]. EVI and NIRv in our study provided similar results in monitoring photosynthetic phenology (Figs. 1-3), consistent with [3] and [24]. NIRv can therefore also act as a proxy of $FAPAR_{chl}$. NIRvP, the product of NIRv and PAR, introduces the limitation of external radiation to NIRv, which can be regarded as a powerful proxy of $APAR_{chl}$, i.e., $FAPAR_{chl} \times PAR = APAR_{chl}$. Another study also found that NIRvP was a

robust proxy for far-red SIF across a wide range of spatial and temporal scales [10]. We depicted the averaged seasonality of GPP (represented by SIF), FAPAR$_{chl}$ (by EVI), APAR$_{chl}$ (by EVI × PAR) and LUE (by SIF / (EVI × PAR)) over the northern DBF. The curves for both FAPAR$_{chl}$ and LUE in spring were similar to the curve for GPP, whilst the curve for APAR$_{chl}$ was very different. In contrast, the curves for APAR$_{chl}$ and GPP in autumn generally overlapped each other, whilst deviations were larger for FAPAR$_{chl}$ and for LUE, specially. These results highlighted that VIs performed differently in tracking GPP across different growth stages.
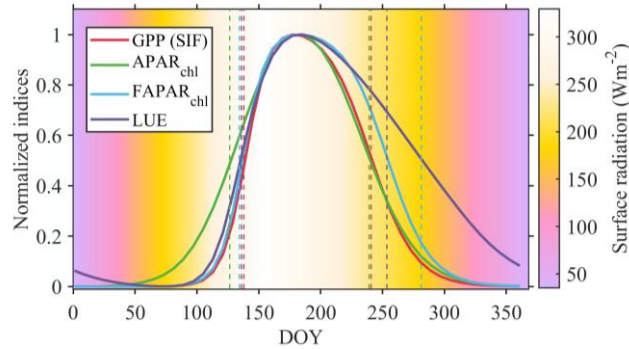
Fig. 4. Seasonality of gross primary productivity (GPP), absorbed photosynthetic active radiation absorbed by chlorophyll (APAR$_{chl}$), fraction of absorbed photosynthetically active radiation absorbed by chlorophyll (FAPAR$_{chl}$) and light-use efficiency (LUE). All indicators were linearly normalized to [0, 1] for visualization. The background colors represent the change of surface radiation. DOY: day of year.

Vegetation needs time to resume primary productivity in spring after leaf-budding by absorbing carbon [5]. The timing of the lag of carbon assimilation behind leaf emergence in spring [25] was thus consistent with the trends of lag of spring SIF behind VI-based spring phenology (Fig. 2 (a)). Vegetation photosynthesis increased with FAPAR$_{chl}$ when available incoming solar radiation was sufficient and temperatures were favorable (Fig. 4), so the content of canopy chlorophyll may be the main factor affecting the phenology, as also reported by [7] that canopy chlorophyll content was strongly correlated with photosynthetic capacity. Photosynthesis always shuts down in autumn before leaf-drop [26], because plant photosynthesis in autumn is limited by the availability of light with the rapid decline of solar radiation.[27]. This shutdown is consistent with our finding that plant photosynthesis decreased as APAR$_{chl}$ decreased (Fig. 4). Insufficient radiation inhibits the physiology of vegetation, i.e., the vegetation cannot use enough light for photosynthesis even though chlorophyll still remains, accounting for the deviation of FAPAR$_{chl}$ from GPP.

Different VIs generally contain different types of information about photosynthesis, so we suggest that VIs should be dedicatedly selected for improving the extraction of photosynthetic phenology. For example, chlorophyll content in spring dominates the rate of carbon sequestration, so VIs containing information about chlorophyll, e.g., EVI and NIRv, can reliably estimate SOS. Low radiation level in autumn and at high latitudes limits canopy photosynthesis. VIs containing information about radiation, e.g., NIRvP, may therefore be the best choice for extracting EOS. The combination of multiple VIs will help to improve our understanding of terrestrial ecosystems and the carbon cycle.

V. Conclusions

We compared the performances of four commonly used VIs, NDVI, EVI, NIRv and NIRvP, in the extraction of the start and end of the photosynthetically active season over northern DBF regions, using SIF results as reference. The LUE paradigm was used to identify the mechanism of the discrepancy in the extracted phenological metrics. For spring, EVI/NIRv-extracted SOS nearly coincided with the initiation of carbon assimilation, but SOS extracted from NIRvP/NDVI had larger deviations compared with that extracted from SIF (6 and 11 d earlier for NDVI and NIRvP, respectively). For autumn, NDVI-derived EOS lagged greatly (42 d) and EVI/NIRv-derived EOS lagged slightly (13/14 d) behind SIF-derived EOS. In comparison, NIRvP approximated SIF very well, with the bias decreasing to only 2 d. The divergent performances of the VIs in extracting photosynthetic phenology indicated that the main factors limiting photosynthesis differed among the stages of growth. VIs associated with FAPAR$_{chl}$, e.g., EVI and NIRv, and VIs associated with APAR$_{chl}$, e.g., NIRvP, are respectively recommended for extracting the timing of the start and end of the photosynthetically active season. Our study will contribute to a better understanding of the divergence in the phenological shifts in greenness and photosynthesis.

VI. Funding

Reference

[1] C. D. Keeling, J. F. S. Chin, and T. P. Whorf, "Increased activity of northern vegetation inferred from atmospheric CO2 measurements," *Nature,* vol. 382, no. 6587, pp. 146-149, Jul, 1996.

[2] T. F. Keenan *et al.*, "Net carbon uptake has increased through warming-induced changes in temperate forest phenology," *Nat. Clim. Chang.,* vol. 4, no. 7, pp. 598-604, Jul, 2014.

[3] G. F. Yin, A. Verger, I. Filella, A. Descals, and J. Penuelas, "Divergent Estimates of Forest Photosynthetic Phenology Using Structural and Physiological Vegetation Indices," *Geophys. Res. Lett.,* vol. 47, no. 18, Sep, 2020.

[4] J. L. Monteith, "Solar Radiation and Productivity in Tropical Ecosystems," *Journal of Applied Ecology,* vol. 9, pp. 747, Dec, 1972.

[5] S. J. Jeong *et al.*, "Application of satellite solar-induced chlorophyll fluorescence to understanding large-scale variations in vegetation phenology and function over northern high latitude forests," *Remote Sens. Environ.,* vol. 190, pp. 178-187, Mar, 2017.

[6] X. M. Xiao, "Light absorption by leaf chlorophyll and maximum light use efficiency," *IEEE Trans. Geosci. Remote Sens.,* vol. 44, no. 7, pp. 1933-1935, Jul, 2006.

[7] H. Croft *et al.*, "Leaf chlorophyll content as a proxy for leaf photosynthetic capacity," *Glob. Change. Biol,* vol. 23, no. 9, pp. 3513-3524, Sep, 2017.

[8] P. D'Odorico *et al.*, "The match and mismatch between photosynthesis and land surface phenology of deciduous forests," *Agric. For. Meteorol.,* vol. 214-215, pp. 25-38, Dec, 2015.

[9] G. Badgley, C. B. Field, and J. A. Berry, "Canopy near-infrared reflectance and terrestrial photosynthesis," *Science Advances,* vol. 3, no. 3, Mar, 2017.

[10] B. Dechant *et al.*, "NIRvP: A robust structural proxy for sun-induced chlorophyll fluorescence and photosynthesis across scales," *Remote Sens. Environ.,* vol. 268, Jan, 2022.

[11] A. Porcar-Castell *et al.*, "Linking chlorophyll a fluorescence to photosynthesis for remote sensing applications: mechanisms and challenges," *J. Exp. Bot.,* vol. 65, no. 15, pp. 4065-4095, Aug, 2014.

[12] T. S. Magney *et al.*, "Mechanistic evidence for tracking the seasonality of photosynthesis with solar-induced fluorescence," *Proc Natl Acad Sci U S A,* vol. 116, no. 24, pp. 11640-11645, Jun, 2019.

[13] C. B. Schaaf *et al.*, "First operational BRDF, albedo nadir reflectance products from MODIS," *Remote Sens. Environ.,* vol. 83, no. 1-2, pp. 135-148, Nov, 2002.

[14] X. Li, and J. F. Xiao, "A Global, 0.05-Degree Product of Solar-Induced Chlorophyll Fluorescence Derived from OCO-2, MODIS, and Reanalysis Data," *Remote Sens.,* vol. 11, no. 5, Mar, 2019.

[15] J. Munoz-Sabater *et al.*, "ERA5-Land: a state-of-the-art global reanalysis dataset for land applications," *Earth Syst. Sci. Data,* vol. 13, no. 9, pp. 4349-4383, Sep, 2021.

[16] S. Bontemps *et al.*, "Multi-year global land cover mapping at 300 m and characterization for climate modelling: achievements of the Land Cover component of the ESA Climate Change Initiative," *Int. Arch. Photogramm. Remote Sens. Spatial Inf. Sci.,* vol. XL-7/W3, pp. 323-328, May, 2015.

[17] J. W. Rouse, R. H. Haas, J. A. Schell, and D. W. Deering, "Monitoring vegetation systems in the Great Plains with ERTS," in 3rd ERTS Symposium, NASA SP-351 I, 1974.

[18] H. Q. Liu, and A. Huete, "A feedback based modification of the NDVI to minimize canopy background and atmospheric noise," *IEEE Trans. Geosci. Remote Sens.,* vol. 33, no. 2, pp. 457-465, Mar, 1995.

[19] P. Jonsson, and L. Eklundh, "TIMESAT - a program for analyzing time-series of satellite sensor data," *Comput Geosci,* vol. 30, no. 8, pp. 833-845, Oct, 2004.

[20] M. F. Garbulsky, I. Filella, A. Verger, and J. Peñuelas, "Photosynthetic light use efficiency from satellite sensors: From global to Mediterranean vegetation," *Environ. Exp. Bot.,* vol. 103, pp. 3-11, Jul, 2014.

[21] R. B. Myneni, and D. L. Williams, "On the relationship between FAPAR and NDVI," *Remote Sens. Environ.,* vol.

49, no. 3, pp. 200-211, Sep, 1994.

[22]   S. W. Running *et al.*, "A continuous satellite-derived measure of global terrestrial primary production," *Bioscience,* vol. 54, no. 6, pp. 547-560, Jun, 2004.

[23]   Y. Zhang *et al.*, "Spatio-Temporal Convergence of Maximum Daily Light-Use Efficiency Based on Radiation Absorption by Canopy Chlorophyll," *Geophys. Res. Lett.,* vol. 45, no. 8, pp. 3508-3519, Apr, 2018.

[24]   C. Wang *et al.*, "Phenology Dynamics of Dryland Ecosystems Along the North Australian Tropical Transect Revealed by Satellite Solar-Induced Chlorophyll Fluorescence," *Geophys. Res. Lett.,* vol. 46, no. 10, pp. 5294-5302, May, 2019.

[25]   K. Kikuzawa, "Phenological and morphological adaptations to the light environment in two woody and two herbaceous plant species," *Functional Ecology,* vol. 17, no. 1, pp. 29-38, Feb, 2003.

[26]   F. Daumard *et al.*, "A Field Platform for Continuous Measurement of Canopy Fluorescence," *IEEE Trans. Geosci. Remote Sens.,* vol. 48, no. 9, pp. 3358-3368, Sep, 2010.

[27]   Y. Zhang, R. Commane, S. Zhou, A. P. Williams, and P. Gentine, "Light limitation regulates the response of autumn terrestrial carbon uptake to warming," *Nat. Clim. Chang.,* vol. 10, no. 8, pp. 739-743, Aug, 2020.

[28]   R. Congalton, J. Gu, K. Yadav, P. Thenkabail, and M. Ozdogan, "Global Land Cover Mapping: A Review and Uncertainty Analysis," *Remote Sens.,* vol. 6, no. 12, pp. 12070-12093, Dec, 2014.